

# Stable switch action based on quantum interference effect

Sreemoyee Mukherjee,\* Ashutosh Yadav,<sup>†</sup> and P. Singha Deo<sup>‡</sup>

*S. N. Bose National Centre for Basic Sciences, Salt Lake, Kolkata 700 098, India*

(Dated: February 20, 2022)

## Abstract

Although devices working on quantum principles can revolutionize the electronic industry, they have not been achieved yet as it is difficult to control their stability. We show that one can use evanescent modes to build stable quantum switches. The physical principles that make this possible is explained in detail. Demonstrations are given using a multichannel Aharonov - Bohm interferometer. We propose a new  $S$  matrix for multichannel junctions to solve the scattering problem.

PACS numbers: 73.23.Ad, 73.21.Hb, 73.63.Nm

## I. INTRODUCTION

Advances in electron beam lithography within the last few years have made it possible to fabricate nano sized or mesoscopic artificial structures with good control over design parameters and probe the quantum transport properties<sup>1</sup>. These include very narrow quasi one-dimensional quantum wires, zero-dimensional electron systems or quantum dots, rings, etc., constructed at a semiconductor interface. Typical sizes of these systems vary between 1 to 10  $\mu\text{m}$ . At very low temperatures (typically mK), the scattering by phonons is significantly suppressed, and the phase coherence length can become large compared to the system size. In this regime the electron maintains the single particle phase coherence across the entire sample. The sample becomes an electron waveguide where the transport properties are solely determined by the impurity configuration and the geometry of the conductor and by the principles of quantum mechanics<sup>1</sup>.

Such advances in mesoscopic structures have led to the possibility of new quantum semiconductor devices. These active quantum devices rely on quantum effects for their operation based on interferometric principles, and are quantum analog of well-known optical and microwave devices<sup>1</sup>. The mechanism of switch action by quantum interference is a new idea in electronic application. Several potential switching devices have been proposed, wherein one controls the relative phase difference between different interfering paths (say, in semiconducting loop structures) by applying electrostatic or magnetic fields<sup>2-4</sup>. The possibility of achieving transistor action in T-shaped structure by varying the effective length of the vertical open ended lead has also been explored<sup>5</sup>. Devices in which electrons carry current without being scattered either elastically or inelastically (ballistic devices) promise to be much faster and will consume less power than the conventional devices. It should also be noted that quantum devices can exhibit multifunctional property (e.g., single stage frequency multiplier) wherein the functions of an entire circuit within a single element can be performed<sup>6</sup>. They can also lead to tremendous down sizing of electronic devices. The conventional transistors operate in a classical diffusive regime and are not very sensitive to variations in material parameters such as dimensions or the presence of small impurities or non-uniformity in size and shape. These devices operate by controlling the carrier density of quasi-particles. However, proposed quantum devices are not very robust in the sense that the operational characteristics depend very sensitively on material parameters, impurity con-

figuration, shape and size, temperature and Fermi energy<sup>7</sup>. For example, incorporation of a single impurity in the mesoscopic device can change, non-trivially, the interference of partial electron waves propagating through the sample, and hence the electron transmission (operational characteristics) across the sample<sup>8</sup>. In such devices the actual problem of control and reproducibility of operating thresholds becomes highly nontrivial. These devices can be exploited if we achieve the technology that can reduce or control the phase fluctuations to a small fraction of  $2\pi$ <sup>9</sup>. A lot of work has been done in one dimensional quantum rings<sup>9-18</sup>. However, the experimental rings are always in two dimension or in three dimension. Such systems have not received much theoretical attention because multichannel junctions are very difficult to account for theoretically. Earlier models either do not account for channel mixing or do not allow the inclusion of evanescent modes.

## II. THEORETICAL ANALYSIS

Fig. 1 represents the schematic diagram of a finite thickness mesoscopic quantum ring under consideration. It is made up of normal metal or semiconductor and electronic transport in such systems can be well described by an effective mass theory<sup>1</sup>. Incident electrons coming from the source reservoir on the left (say), gets scattered by the ring. Division of wave front occurs at junction  $J1$ ; a partial wave propagates along the upper arm of the ring and another partial wave propagates along the lower arm of the ring. These two partial waves recombine and give a transmittance that bears the signature of interference between the two partial waves along the two arms of the ring. This interference can be modified by an Aharonov - Bohm flux through the center of the ring. The description of the figure is given in further detail in the figure caption.

The Schrödinger equation for a quasi one dimensional wire is (the third degree of freedom, i.e., z-direction, is usually frozen by creating a strong quantization<sup>1</sup>)

$$-\frac{\hbar^2}{2m^*}\left(\frac{\partial^2\psi}{\partial x^2} + \frac{\partial^2\psi}{\partial y^2}\right) + V(x, y)\psi(x, y) = E\psi(x, y) \quad (1)$$

Here the  $x$  coordinate is along the wire,  $y$  coordinate is perpendicular to it,  $m^*$  is the electron effective mass and  $E$  is the electron energy. In region I and IV (see Fig. 1) we have only the confinement potential. That is

$$V(x, y) = V(y).$$

Whereas in region II and III apart from the confinement potential we take a constant potential  $V_0$  that can be used to excite evanescent modes inside the ring. That is

$$V(x, y) = V(y) + V_0.$$

Without any loss of generality we take  $V(y)$  to be an infinite square well potential. That is

$$V(y) = 0 \quad \text{for } -a/2 \leq y \leq a/2$$

and

$$V(y) = \infty \quad \text{for } |y| > a/2 \tag{2}$$

The width of the quantum wire is  $a$ . The wave functions in the ring can be obtained by solving Eq. (1) where we assume the ring to be so large compared to the de Broglie wave length that its curvature can be neglected<sup>19</sup>. The length of the ring is  $L = l_1 + l_2$ , where  $l_1$  is the length of the upper arm and  $l_2$  is the length of the lower arm. The magnetic field appears just as a phase of  $\psi(x, y)$  and will be accounted for while applying the boundary conditions<sup>20</sup>. In regions I and IV Eq. (1) can be separated as

$$\psi(x, y) = \phi(x)\xi(y) \tag{3}$$

to give

$$-\frac{\hbar^2}{2m^*} \frac{\partial^2 \phi(x)}{\partial x^2} = \frac{\hbar^2 k^2}{2m^*} \phi(x) \tag{4}$$

and

$$-\frac{\hbar^2}{2m^*} \frac{\partial^2 \xi(y)}{\partial y^2} + V(y)\xi(y) = \varepsilon \xi(y) \tag{5}$$

Since  $V(y)$  is a square well potential of width  $a$ , Eq. (5) gives

$$\xi_n(y) = \sin \frac{n\pi}{a} \left( \frac{a}{2} + y \right) \tag{6}$$

and

$$\varepsilon_n = \frac{n^2 \pi^2 \hbar^2}{2m^* a^2} \tag{7}$$

Eq. (4) has solution of the form

$$\phi_n(x) = e^{\pm i k_n x}$$

with

$$k_n = \sqrt{\frac{2m^* E}{\hbar^2} - \frac{n^2 \pi^2}{a^2}} \tag{8}$$

or

$$E = \varepsilon_n + \frac{\hbar^2 k_n^2}{2m^*} \quad (9)$$

So wave functions in different regions I and IV can be written as

$$\psi_I^{(1)} = \left( \frac{e^{ik_1x}}{\sqrt{k_1}} + \frac{r'_{11}e^{-ik_1x}}{\sqrt{k_1}} \right) \sin \frac{\pi}{a} \left( y + \frac{a}{2} \right) \quad (10)$$

$$\psi_I^{(2)} = \left( \frac{r'_{12}e^{-ik_2x}}{\sqrt{k_2}} \right) \sin \frac{2\pi}{a} \left( y + \frac{a}{2} \right) \quad (11)$$

$$\psi_{IV}^{(1)} = \left( \frac{t'_{11}e^{ik_1x}}{\sqrt{k_1}} \right) \sin \frac{\pi}{a} \left( y + \frac{a}{2} \right) \quad (12)$$

$$\psi_{IV}^{(2)} = \left( \frac{t'_{12}e^{ik_2x}}{\sqrt{k_2}} \right) \sin \frac{2\pi}{a} \left( y + \frac{a}{2} \right) \quad (13)$$

$\psi_I^{(1)}$  is the wave function of region I in channel  $n = 1$  and so on. From Eq. (II), in the first mode

$$k_1 = \sqrt{\frac{2m^*E}{\hbar^2} - \frac{\pi^2}{a^2}} \quad (14)$$

is the propagating wave vector and in the second mode

$$k_2 = \sqrt{\frac{2m^*E}{\hbar^2} - \frac{4\pi^2}{a^2}} \quad (15)$$

is the propagating wave vector. For

$$\frac{4\pi^2}{a^2} < E < \frac{9\pi^2}{a^2} \quad (16)$$

both  $k_1$  and  $k_2$  are real as can be seen from Eq. (14) and Eq. (15) and  $k_n$  for  $n > 2$  are imaginary as can be seen from Eq. (II) implying that there are two propagating channels. In the leads we can not have evanescent modes<sup>21,22</sup>. Now for the region II and region III the potential is  $V(x, y) = V(y) + V_0$ . Wave functions in these regions can be similarly written as

$$\psi_{II}^{(1)} = \left( \frac{A_1e^{iq_1x}}{\sqrt{q_1}} + \frac{B_1e^{-iq_1x}}{\sqrt{q_1}} \right) \sin \frac{\pi}{a} \left( y + \frac{a}{2} \right) \quad (17)$$

$$\psi_{II}^{(2)} = \left( \frac{A_2e^{iq_2x}}{\sqrt{q_2}} + \frac{B_2e^{-iq_2x}}{\sqrt{q_2}} \right) \sin \frac{2\pi}{a} \left( y + \frac{a}{2} \right) \quad (18)$$

$$\psi_{III}^{(1)} = \left( \frac{C_1e^{iq_1x}}{\sqrt{q_1}} + \frac{D_1e^{-iq_1x}}{\sqrt{q_1}} \right) \sin \frac{\pi}{a} \left( y + \frac{a}{2} \right) \quad (19)$$

$$\psi_{III}^{(2)} = \left( \frac{C_2e^{iq_2x}}{\sqrt{q_2}} + \frac{D_2e^{-iq_2x}}{\sqrt{q_2}} \right) \sin \frac{2\pi}{a} \left( y + \frac{a}{2} \right) \quad (20)$$

In these regions the energy can be similarly written as

$$E - V_0 = \frac{\hbar^2 q_n^2}{2m^*} + \frac{n^2 \pi^2 \hbar^2}{2m^* a^2}$$

or

$$q_n = \sqrt{\frac{2m^*(E - V_0)}{\hbar^2} - \frac{n^2 \pi^2}{a^2}}$$

Hence, in the first mode

$$q_1 = \sqrt{\frac{2m^*(E - V_0)}{\hbar^2} - \frac{\pi^2}{a^2}} \quad (21)$$

is the wave vector and in the second mode

$$q_2 = \sqrt{\frac{2m^*(E - V_0)}{\hbar^2} - \frac{4\pi^2}{a^2}} \quad (22)$$

is the wave vector. Depending on the choice of energy  $E$  and potential  $V_0$ ,  $q_1$  and  $q_2$  can be real (propagating mode) as well as imaginary (evanescent mode). Such evanescent states can always be excited in the internal regions of the system but not in leads<sup>21,22</sup>.

### *S - matrix for the Junction*

Earlier works have proposed junction  $S$  matrix for solving the scattering problem of a ring<sup>10–17,23,24</sup> where the following conditions are satisfied at the junction: (a) conservation of current, (b) continuity of wave function and (c) unitarity of  $S$  matrix. However, earlier models do not account for channel mixing and also do not allow us to include evanescent modes. We give below a simple way to obtain an  $S$  matrix for a 3 legged two channel junction shown in Fig. 2, that satisfy the three conditions stated above. For our junction  $S$  matrix channel mixing occurs and evanescent modes can also be accounted for. The approach can be generalized to any numbers of channels.

Fig. 2 represents schematic diagram of a 3 legged scatterer that we find at  $J1$  or  $J2$  of Fig. 1. All the legs or leads are made up of normal metal or semiconductor. Incident electrons coming from the left of the lead labeled I, gets scattered at the junction where the three leads meet. Division of wave front occurs and partial waves propagate along the upper arm labeled II and along the lower arm labeled III. The wave functions of the electron in different regions are again obtained from Eq. (1) and shown in their respective places for two propagating channels in each lead. Potential in region I (stripped region) is zero whereas potential in regions II and III (shaded region) is  $V_0$ .

Taking the clue from reflection and transmission amplitudes for a one dimensional step potential<sup>25</sup> we can write for the different reflection amplitudes  $r_{mn}$  and transmission amplitudes  $f_{mn}$  and  $g_{mn}$  shown in Fig. 2 as

$$\begin{aligned}
r_{11} &= \left( \frac{k_1 - k_2 - 2q_1 - 2q_2}{k_1 + k_2 + 2q_1 + 2q_2} \right) \\
r_{12} &= \left( \frac{2\sqrt{k_1 k_2}}{k_1 + k_2 + 2q_1 + 2q_2} \right) \\
f_{11} = g_{11} &= \left( \frac{2\sqrt{k_1 q_1}}{k_1 + k_2 + 2q_1 + 2q_2} \right) \\
f_{12} = g_{12} &= \left( \frac{2\sqrt{k_1 q_2}}{k_1 + k_2 + 2q_1 + 2q_2} \right) \\
r_{22} &= \left( \frac{k_2 - k_1 - 2q_1 - 2q_2}{k_1 + k_2 + 2q_1 + 2q_2} \right) \\
r_{21} &= \left( \frac{2\sqrt{k_1 k_2}}{k_1 + k_2 + 2q_1 + 2q_2} \right) \\
f_{21} = g_{21} &= \left( \frac{2\sqrt{k_2 q_1}}{k_1 + k_2 + 2q_1 + 2q_2} \right) \\
f_{22} = g_{22} &= \left( \frac{2\sqrt{k_2 q_2}}{k_1 + k_2 + 2q_1 + 2q_2} \right)
\end{aligned}$$

$S$  matrix for the junction  $S_j$  is therefore

$$S_j = \begin{bmatrix} r_{11} & r_{12} & f_{11} & f_{12} & g_{11} & g_{12} \\ r_{21} & r_{22} & f_{21} & f_{22} & g_{21} & g_{22} \\ f_{11} & f_{12} & r_{11} & r_{12} & g_{11} & g_{12} \\ f_{21} & f_{22} & r_{21} & r_{22} & g_{21} & g_{22} \\ g_{11} & g_{12} & g_{11} & g_{12} & r_{11} & r_{12} \\ g_{21} & g_{22} & g_{21} & g_{22} & r_{21} & r_{22} \end{bmatrix} \quad (23)$$

One can check that the following conditions of unitarity are satisfied

$$|r_{11}|^2 + |r_{12}|^2 + |f_{11}|^2 + |f_{12}|^2 + |g_{11}|^2 + |g_{12}|^2 = 1 \quad (24)$$

$$|r_{22}|^2 + |r_{21}|^2 + |f_{21}|^2 + |f_{22}|^2 + |g_{21}|^2 + |g_{22}|^2 = 1 \quad (25)$$

The ring wave functions and the lead wave functions at the junction  $J1$  of Fig. 1 can be matched as

$$\begin{pmatrix} \frac{r'_{11}}{\sqrt{k_1}} \\ \frac{r'_{12}}{\sqrt{k_2}} \\ \frac{A_1}{\sqrt{q_1}} \\ \frac{A_2}{\sqrt{q_2}} \\ \frac{D_1 e^{-iq_1 l_2}}{\sqrt{q_1}} \\ \frac{D_2 e^{-iq_2 l_2}}{\sqrt{q_2}} \end{pmatrix} = S_j \begin{pmatrix} \frac{1}{\sqrt{k_1}} \\ 0 \\ \frac{B_1 e^{-i\alpha}}{\sqrt{q_1}} \\ \frac{B_2 e^{-i\alpha}}{\sqrt{q_2}} \\ \frac{C_1 e^{iq_1 l_2 + i\beta}}{\sqrt{q_1}} \\ \frac{C_2 e^{iq_2 l_2 + i\beta}}{\sqrt{q_2}} \end{pmatrix} \quad (26)$$

Similarly one can match the wavefunctions at the junction  $J2$  to give a set of equations given below

$$1 + r'_{11} - \sqrt{\frac{k_1}{q_1}} A_1 - \sqrt{\frac{k_1}{q_1}} B_1 e^{-i\alpha} = 0 \quad (27)$$

$$r'_{12} - \sqrt{\frac{k_2}{q_2}} A_2 - \sqrt{\frac{k_2}{q_2}} B_2 e^{-i\alpha} = 0 \quad (28)$$

$$1 + r'_{11} - \sqrt{\frac{k_1}{k_2}} r'_{12} = 0 \quad (29)$$

$$1 + r'_{11} - \sqrt{\frac{k_1}{q_1}} C_1 e^{iq_1 l_2 + i\beta} - \sqrt{\frac{k_1}{q_1}} D_1 e^{-iq_1 l_2} = 0 \quad (30)$$

$$r'_{12} - \sqrt{\frac{k_2}{q_2}} C_2 e^{iq_2 l_2 + i\beta} - \sqrt{\frac{k_2}{q_2}} D_2 e^{-iq_2 l_2} = 0 \quad (31)$$

$$\begin{aligned} ik_1 - ik_1 r'_{11} - iq_1 \sqrt{\frac{k_1}{q_1}} A_1 + iq_1 \sqrt{\frac{k_1}{q_1}} B_1 e^{-i\alpha} - iq_2 \sqrt{\frac{k_1}{q_2}} A_2 + \\ iq_2 \sqrt{\frac{k_1}{q_2}} B_2 e^{-i\alpha} - iq_1 \sqrt{\frac{k_1}{q_1}} C_1 e^{iq_1 l_2 + i\beta} - iq_1 \sqrt{\frac{k_1}{q_1}} D_1 e^{-iq_1 l_2} + \\ iq_2 \sqrt{\frac{k_1}{q_2}} C_2 e^{iq_2 l_2 + i\beta} - iq_2 \sqrt{\frac{k_1}{q_2}} D_2 e^{-iq_2 l_2} - ik_2 \sqrt{\frac{k_1}{k_2}} r'_{12} = 0 \end{aligned} \quad (32)$$

$$t'_{11} - \sqrt{\frac{k_1}{q_1}} A_1 e^{iq_1 l_1 + i\alpha} - \sqrt{\frac{k_1}{q_1}} B_1 e^{-iq_1 l_1} = 0 \quad (33)$$

$$t'_{12} - \sqrt{\frac{k_2}{q_2}} A_2 e^{iq_2 l_1 + i\alpha} - \sqrt{\frac{k_2}{q_2}} B_2 e^{-iq_2 l_1} = 0 \quad (34)$$

$$t'_{11} - \sqrt{\frac{k_1}{k_2}} t'_{12} = 0 \quad (35)$$

$$t'_{11} - \sqrt{\frac{k_1}{q_1}}C_1 - \sqrt{\frac{k_1}{q_1}}D_1e^{-i\beta} = 0 \quad (36)$$

$$t'_{12} - \sqrt{\frac{k_2}{q_2}}C_2 - \sqrt{\frac{k_2}{q_2}}D_2e^{-i\beta} = 0 \quad (37)$$

$$\begin{aligned} & iq_1\sqrt{\frac{k_1}{q_1}}A_1e^{iq_1l_1+i\alpha} - iq_1\sqrt{\frac{k_1}{q_1}}B_1e^{-iq_1l_1} + iq_2\sqrt{\frac{k_1}{q_2}}A_2e^{iq_2l_1+i\alpha} - \\ & iq_2\sqrt{\frac{k_1}{q_2}}B_2e^{-iq_2l_1} - iq_1\sqrt{\frac{k_1}{q_1}}C_1 + iq_1\sqrt{\frac{k_1}{q_1}}D_1e^{i\beta} - iq_2\sqrt{\frac{k_1}{q_2}}C_2 + \\ & iq_2\sqrt{\frac{k_1}{q_2}}D_2e^{-i\beta} - ik_1t'_{11} - ik_2\sqrt{\frac{k_1}{k_2}}t'_{12} = 0 \end{aligned} \quad (38)$$

Solving them we can find the  $S$  matrix elements  $r'_{11}$ ,  $r'_{12}$ ,  $t'_{11}$  and  $t'_{12}$  for the Aharonov - Bohm ring.

### III. RESULTS AND DISCUSSIONS

Here we are considering two channel Aharonov - Bohm ring that are characterized by four transmission amplitudes  $t'_{11}$ ,  $t'_{12}$ ,  $t'_{21}$  and  $t'_{22}$  and four reflection amplitudes  $r'_{11}$ ,  $r'_{12}$ ,  $r'_{21}$  and  $r'_{22}$ . Landauer's formula gives the two probe conductance  $G$  as

$$G = \frac{2e^2}{h} \sum_{i,j} |t'_{ij}|^2. \quad (39)$$

The transmission amplitude from mode  $j$  to mode  $i$  is  $t'_{ij}$ .  $G$  is a strongly oscillating function of  $\phi/\phi_0$  implying we can use flux to drive the system from a conducting state to an insulating state that can be identified with 1 and 0 of a switch as will be exemplified. Such a switch will therefore be working entirely on quantum mechanical principles. Such devices if achieved will be a major technological break through. First of all, it will transcend Moore's law by leaps and bounds to result in extremely small devices. Secondly, such devices will consume very little power and will solve the problem of present day computers dissipating a lot of energy and getting heated up. Other advantages are mentioned in introduction. However, such devices have not been achieved so far because switches based on quantum interference principles as the one we are discussing here in our work are not stable<sup>7</sup>. Small changes in temperature or incorporation of a single impurity can drastically change the operational characteristics of the switch. One can understand this in terms of the fact that impurity

cause additional reflections or temperature increases Fermi energy and hence wavelength and therefore imply changes in path lengths in an interference set up. We demonstrate below how changes in path lengths can drastically alter the operational characteristics of an Aharonov - Bohm ring. Finally we will show that there is a solution to the problem.

In Fig. 3, we show  $\frac{G}{2e^2/h}$  for a two channel Aharonov-Bohm ring with  $l_1/a = 5$ ,  $l_2/a = 5$  (solid line) and with  $l_1/a = 4$ ,  $l_2/a = 6$  (dotted line). We choose incident energy in the range given by Eq. (16) and so we are considering a two channel scattering problem. We take the potential inside the ring  $V_0$  to be 0 implying that both channels are propagating inside the ring. Solid line shows two conductance minima, one is shallow at flux  $\phi/\phi_0 = 0$  (approx) and another is deep at flux  $\phi/\phi_0 = 3.1$  (approx) and it also shows one conductance maximum at flux  $\phi/\phi_0 = 2.4$  (approx). Dotted line also shows two conductance minima, one is shallow at flux  $\phi/\phi_0 = 0$  (approx) and another is deep at flux  $\phi/\phi_0 = 3.1$  (approx) and it shows one conductance maximum at flux  $\phi/\phi_0 = 1.0$  (approx). We can assign the conductance minima as off state and conductance maxima as on state of a switch. Fig. 3 shows that with changing the arm length the minima is not shifting but maxima is shifting a lot. The shallow minima for dotted line is so shallow that it may not be observed in measurement. Much more non-systematic behavior will be shown in subsequent plots. Now we will plot the individual  $|t'_{ij}|^2$  s as a function of  $\phi/\phi_0$  and shown in Fig. 4.

All the plots of individual partial scattering cross sections ( $|t'_{11}|^2$ ,  $|t'_{12}|^2 = |t'_{21}|^2$  and  $|t'_{22}|^2$ ) are qualitatively same as the plot of  $\sum_{i,j} |t'_{ij}|^2$  as a function of  $\phi/\phi_0$ . Peaks are expected to occur at resonance<sup>26</sup> when integral wave numbers fit into the total length of the Aharonov - Bohm ring. However in presence of channel mixing the two channels are not independent. Resonance in one channel builds up density of states in the other channel and so  $|t'_{11}|^2$ ,  $|t'_{12}|^2$ ,  $|t'_{21}|^2$  and  $|t'_{22}|^2$  peak at same flux values. Conductance is determined by the addition of these individual scattering cross sections. Since they are qualitatively same they add up coherently. When all these partial scattering cross sections are coherently added the difference between the on state and the off state becomes 100% for deep minima and it is 50 % for shallow minima in case of solid line in Fig. 3, while it is only 40% for deep minima and 12% for shallow minima in case of dotted line in Fig. 3. Such variations in magnitudes of drops in conductance apart from variations in peak positions already discussed indicates that it is not so efficient to make stable switches.

In Fig. 5, we show  $\frac{G}{2e^2/h}$  for a two channel Aharonov-Bohm ring with  $l_1/a = 5$ ,  $l_2/a = 5$

(solid line) and with  $l_1/a = 3$ ,  $l_2/a = 7$  (dotted line). Again we choose energy in the range given by Eq. (16). However now we also take a non zero electrostatic potential  $V_0$  inside the ring such that  $q_1$  is real and  $q_2$  is imaginary (see Eq. (21) and Eq. (22)). In other words one channel is propagating and the other is evanescent. We have checked that such a situation result in just as much diversity as that with two propagating modes. Here we demonstrate one particular case and give arguments why the behavior is general. Solid line shows two conductance minima and one conductance maximum like the solid line in Fig. 3. It has first a shallow minimum and then has a deep minimum similar to solid line in Fig. 3. Dotted line shows two conductance minima and one conductance maximum like the dotted line in Fig. 3. Here one that was shallow minimum in Fig. 3 has become a deep minimum and the one that was deep minimum in Fig. 3 has become shallow minimum. Unlike in Fig. 3, there is wave propagation in only one channel and since the other channel is evanescent, it has no wave propagation. Peaks occur for propagating channel when integral wave number fits into the total length of the ring<sup>26</sup>. But here we can see  $|t'_{22}|^2$  peak at same flux values as  $|t'_{11}|^2$  because again in presence of channel mixing the two modes are not independent. Resonance in the propagating channel boost up density of states in the evanescent channel and hence the evanescent channel also becomes highly conducting. Thus the diversity results from the random behavior of the propagating channel. We show the individual  $|t'_{ij}|^2$ s corresponding to Fig. 5 in Fig. 6. They are again qualitatively same as the curves obtained in Fig. 5 which means the individual components add up coherently just as it happened for two propagating modes. Conduction along the evanescent mode is equally strong and diverse due to the presence of the propagating mode.

In Fig. 7, we show  $\frac{G}{2e^2/h}$  for a two channel Aharonov-Bohm ring with  $l_1/a = 5$ ,  $l_2/a = 5$  (solid line) and with  $l_1/a = 4$ ,  $l_2/a = 6$  (dotted line). Incident energy and the electrostatic potential are so chosen that like in Fig. 5 one channel is propagating and another is evanescent. Solid line shows one conductance maximum and one conductance minimum instead of two conductance minima seen in earlier figures. Only difference is that we have slightly changed the energy of the incoming electrons from  $E = \frac{45\hbar^2}{m^*a^2}$  (Fig. 5) to  $E = \frac{47\hbar^2}{m^*a^2}$  (Fig. 7) keeping  $l_1, l_2$  same. Dotted line shows two conductance minima and one conductance maximum. The drops of two minima are comparable which gives the appearance of a  $\phi_0/2$  periodicity. This is unlike what we saw in earlier figures. Here too all the plots of individual partial scattering cross sections are qualitatively same as the plot of  $\sum_{i,j} |t'_{ij}|^2$  as a function

of  $\phi/\phi_0$  and so not shown.

The random behavior of conductance changes when we make both the modes to be evanescent. An electron in an evanescent mode do not acquire phase changes associated with propagation. Only phase changes are due to Aharonov - Bohm effect and we find that within a period (0 to  $2\pi$ ) conductance is maximum at zero flux, then it goes through a deep minima and rise again to a maximum value. One can explain this as follows. Conductance being a symmetric function of flux (Onsager reciprocity relation), is a function of  $(\cos n\phi/\phi_0)$ . So it maximizes at 0 flux and then decreases with flux. Periodicity is always  $\phi_0$  in absence of other competing source of phase changes and absence of resonances. This behavior is independent of all parameters as will be demonstrated below. However since evanescent modes are not very conducting we have to take smaller rings to get same order of magnitude in conductance variations as that of propagating modes. But the magnitude can be enhanced by taking a ring that can support many evanescent modes.

In Fig. 8, we have taken many choices of arm length and we have seen that there is only one conductance maxima at flux  $\phi/\phi_0 = 0$  (approx) and only one conductance minima at flux  $\phi/\phi_0 = 2.5$  (approx). Thus, here the behavior remains uniform with changing the arm length. Conductance variation from maximum to minimum is 82%. The individual  $|t'_{ij}|^2$  s as a function of  $\phi/\phi_0$  shows similar behavior as that of Fig. 8 and shown in Fig. 9. In case of Fig. 9(a), conductance drops by 38%, in case of Fig. 9(b), conductance drops by 18% and for Fig. 9(c), conductance drops by 8%. When different channels add up coherently percentage drop of conductance becomes 82%. By using larger and larger number of evanescent channels percentage drop in conductance can thus be enhanced and efficiency of switch can be increased.

It is not always possible to maintain the incidence energy ( $\frac{Em^*a^2}{\hbar^2}$ ) values constant due to statistical fluctuation in voltage of the battery or due to temperature changes. Now we will plot  $\sum_{i,j} |t'_{ij}|^2$  as a function of  $\phi/\phi_0$  for different  $\frac{Em^*a^2}{\hbar^2}$  values and we will show that the behavior is also independent of incident energy when we employ evanescent modes. This is not the case with propagating modes where changes of incident energy result in just as much diversity that we get on changing  $l_1$  and  $l_2$  and hence not shown here. In Fig. 10, two values of incident energy and electrostatic potential are so chosen that both channels are evanescent. Here again we find that  $\sum_{i,j} |t'_{ij}|^2$  as a function of  $\phi/\phi_0$  is roughly independent of incident energy and the drop is almost 75-80%. Since in the evanescent mode switching

action is independent of all parameters, switch can become stable, efficient and robust

So far we have considered two propagating, one propagating - one evanescent and two evanescent modes separately. For all these cases the total ring length were the same, we only changed the relative ratio of arm lengths. In these cases we have shown that when there are propagating modes then the peaks are shifting and the depth of the valleys are changing from shallow to deep. Resonances are determined by the total ring length. If we consider cases where the total ring length does not remain same then one can get even more diverse behavior.

In Fig. 11 we have considered both the channels to be propagating with two choices of  $(l_1 + l_2)$ . We have shown here that resonance position of the solid line is different from the resonance position of the dotted line. The solid line has a valley where the dotted line has a peak. But again if we use evanescent modes then changes in total ring length can not result in diverse behavior.

In Fig. 12 we have considered both the channels to be evanescent with two choices of  $(l_1 + l_2)$ . Here the nature of the solid curve and the dotted curve are the same as that obtained so far. We have shown in previous figures that if we use evanescent modes, conductance does not depend on the relative ratios of arm lengths and Fermi energy and in this Fig. 12 we have shown that the conductance also does not depend on the total ring length of the Aharonov - Bohm ring.

#### IV. CONCLUSIONS

In this work we have studied two channel (transverse modes) Aharonov - Bohm ring. When we consider both the channels to be propagating then we have shown that if we change the parameters such as the total ring length, relative ratio of arm lengths, Fermi energy etc., the behavior of the conductance becomes diverse in nature in different cases. Similar situation arises if we take one propagating and one evanescent modes. In presence of channel mixing the modes are not independent. Resonance in the propagating channel boost up density of states in the evanescent channel and hence the evanescent channel also becomes highly conducting. Such diverse behavior supports Landauer's claim that switch action based on interference principle are not stable and practical. Finally we have considered both the modes to be evanescent along the Aharonov - Bohm ring. Here we

have found that conductance is qualitatively as well as quantitatively same for all variations in parameters like total ring length, relative ratio of arm lengths, Fermi energy etc. We can obtain appreciable changes in conductance when using evanescent modes. Different channels add up coherently and so by using larger and larger number of evanescent channels we can enhance the percentage drop in conductance and hence efficiency of the switch. Change in impurity configuration effectively changes the total ring length and the relative ratio of arm lengths. Rise or drop in temperature effectively changes Fermi energy and hence wavelength. Therefore, conductance behavior will be same if we change the impurity configuration or temperature when we use evanescent modes. Propagation is associated with phase changes which do not arise in case of evanescent modes. In evanescent modes, phase changes are due to Aharonov - Bohm effect only. Periodicity is always  $\phi_0$  in absence of other competing source of phase changes. Conductance being a symmetric function of flux is a function of  $\cos(n\phi/\phi_0)$ . Therefore within a period (0 to  $2\pi$ ) conductance is maximum at zero flux, then it goes through a deep minimum and rise again to a maximum value. We can assign the conductance maximum as on state and conductance minimum as off state of a switch signifying 1 and 0 operation in Boolean algebra. Thus we can conclude that if we employ evanescent modes only, we may be able to build stable, efficient and robust quantum switches.

Earlier works have proposed possibility of switch action with other geometric configurations apart from Aharonov - Bohm ring such as T - shaped structure<sup>5</sup> etc. We may also expect that if we employ evanescent modes in other geometries, conductance will be independent of sample parameters. This is because propagation along evanescent channels are not associated with phase changes. Phase changes can only be induced by external stimuli which is electrostatic potential in case of Ref 5.

### **acknowledgment**

One of us (PSD) would like to thank Prof. A. M. Jayannavar for useful discussions.

---

\* Electronic address: sree.mukherjee@bose.res.in

† Electronic address: ashutoshauchem@gmail.com

<sup>‡</sup> Electronic address: deo@bose.res.in

- <sup>1</sup> S. Datta, *Electronic Transport in Mesoscopic Systems* (Cambridge: Cambridge University Press).
- <sup>2</sup> S. Datta, M. R. Melloch, S. Bandyopadhyay, R. Noren, M. Vaziri, M. Miller and R. Reifenberger. *Phys. Rev. Lett* **55**, 2344(1985); S. Datta, M. R. Melloch, S. Bandyopadhyay, and M. S. Lundstrom, *Appl. Phys. Lett* **48**, 487 (1986).
- <sup>3</sup> S. Datta and B. Das, *Appl. Phys. Lett* **56**, 665 (1990).
- <sup>4</sup> S. Datta and M. J. McLennan, *Rep. Prog. Phys.* **53**, 1003(1990).
- <sup>5</sup> F. Sols, M. Macucci, V. Ravoili, and K. Hess, *Appl. Phys. Lett.*, **54**, 350 (1990); *J. Appl. Phys.* **66**, 3892 (1989).
- <sup>6</sup> S. Subramaniam, S. Bandopadhyay, and W. Porod, *J. Appl. Phys.* **68**, 4861(1990).
- <sup>7</sup> R. Landauer, *Physics Today* **42**, 10, 119(1989).
- <sup>8</sup> B. C. Gupta, P. Singha Deo and A. M. Jayannavar, *Int. J. Mod. Phys. B* **10** 3595(1996).
- <sup>9</sup> A. M. Jayannavar and P. Singha Deo, *Mod. Phys. Lett B* **8**, 301(1994).
- <sup>10</sup> B. Molnár, F. M. Peeters and P. Vasilopoulos, *Phys. Rev B* **69**, 155335(2004).
- <sup>11</sup> B. Molnár, P. Vasilopoulos and F. M. Peeters, *Appl. Phys. Lett* **85**, 4 (2004).
- <sup>12</sup> P. Földi, B. Molnár, M. G. Benedict and F. M. Peeters, *Phys. Rev B* **71**, 033309(2005).
- <sup>13</sup> B. Molnár, P. Vasilopoulos and F. M. Peeters, *Phys. Rev B* **72**, 075330(2005).
- <sup>14</sup> P. Földi, O. Kálmán, M. G. Benedict, and F. M. Peeters, *Phys. Rev B* **73**, 155325(2006).
- <sup>15</sup> P. Vasilopoulos, O. Kálmán, F. M. Peeters, and M. G. Benedict, *Phys. Rev B* **75**, 035304(2007).
- <sup>16</sup> O. Kálmán, P. Földi, M. G. Benedict, F. M. Peeters, *Physica E* **40**, 567(2008).
- <sup>17</sup> S. K. Joshi, D. Sahoo and A. M. Jayannavar, *Phys. Rev B* **64**, 075320(2001).
- <sup>18</sup> C. Benjamin and A. M. Jayannavar, *Int. J. Mod. Phys. B* **16**, 1787(2002).
- <sup>19</sup> S. Sengupta Chowdhury, P. Singha Deo, A. K. Roy and M. Manninen, *New Journal of Physics* **10**, 083014(2008).
- <sup>20</sup> H. F. Cheung, Y. Gefen, E. K. Riedel, and W. H. Shih, *Phys. Rev B* **37**, 6050(1988).
- <sup>21</sup> B. J. van Wees, H. van Houten, C. W. J. Beenakker, J. G. Williamson, L. P. Kouwenhoven, D. van der Marel, and C. T. Foxon, *Phys. Rev. Lett.* **60**, 848(1988).
- <sup>22</sup> D. A. Wharam, T. J. Thornton, R. Newbury, M. Pepper, H. Ahmed, J. E. Frost, D. G. Hasko, D. C. Peacock, D. A. Ritchie, and G. A. C. Jones, *J. Phys. C* **21** L209(1988).
- <sup>23</sup> M. Büttiker, *Phys. Rev. B*, **32**, 1846(1985).

<sup>24</sup> M. Büttiker, Y. Imry, R. Landauer, and S. Pinhas *Phys. Rev. B* **311**, 6207(1985).

<sup>25</sup> E. Merzbacher, *Quantum Mechanics*, 3rd ed. (Wiley, New York, 1997).

<sup>26</sup> H. M. Pastawski, A. Rojo and C. Balseiro, *Phys. Rev B* **37**, 6246(1988).

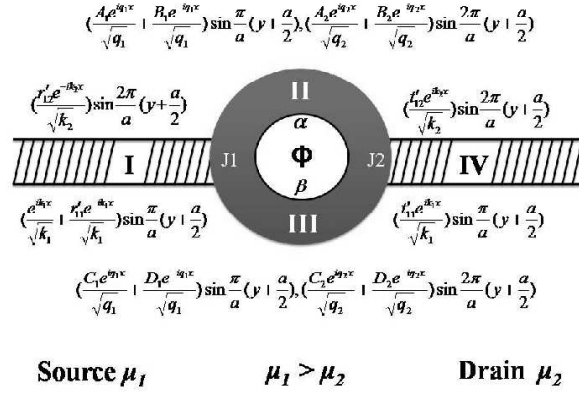


FIG. 1: A finite thickness quantum ring of width  $a$  made up of normal metal or semiconductor is indicated by the grey region. On either sides the quantum ring is attached with quantum wires made up of normal metal or semiconductor. It is indicated by the striped regions. On the left of the above system there is the source reservoir whose chemical potential is  $\mu_1$  and on the right there is the drain reservoir whose chemical potential is  $\mu_2$ . A potential difference  $(\mu_1 - \mu_2)$  between the source reservoir and the drain reservoir drives a transport current. The wave functions of the electron in different regions is shown in the figure at their respective places. Different regions are marked as I, II, III and IV. The ring is pierced by an Aharonov - Bohm flux  $\phi$ .  $\alpha$  is the Aharonov-Bohm phase an electron picks up in region II and  $\beta$  is that in region III.  $J1$  is the junction where the regions I, II and III meets and  $J2$  is the junction where the regions II, III and IV meets.

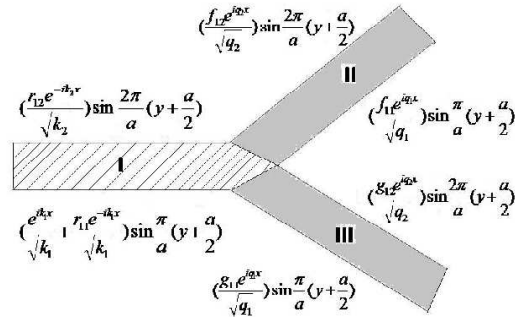


FIG. 2: A three-legged two-channel junction that exists at  $J1$  and  $J2$  of Fig. 1

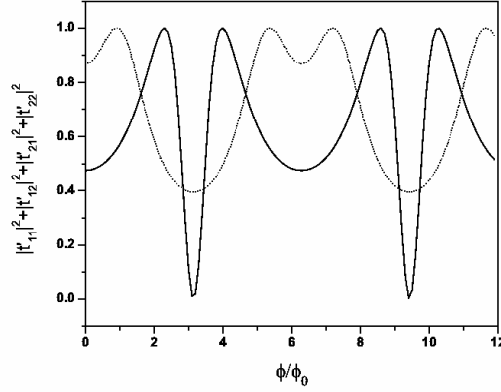


FIG. 3: The figure shows a plot of  $\sum_{i,j} |t'_{ij}|^2$  as a function of  $\phi/\phi_0$ . Here  $\phi_0 = hc/e$ . The incoming electrons have energy  $E = \frac{55\hbar^2}{m^*a^2}$  and the constant potential  $V_0$  of the ring is 0. We are considering in this case two propagating modes. The solid line is  $\sum_{i,j} |t'_{ij}|^2$  for  $l_1/a = 5$ ,  $l_2/a = 5$  and the dotted line is  $\sum_{i,j} |t'_{ij}|^2$  for  $l_1/a = 4$ ,  $l_2/a = 6$ .

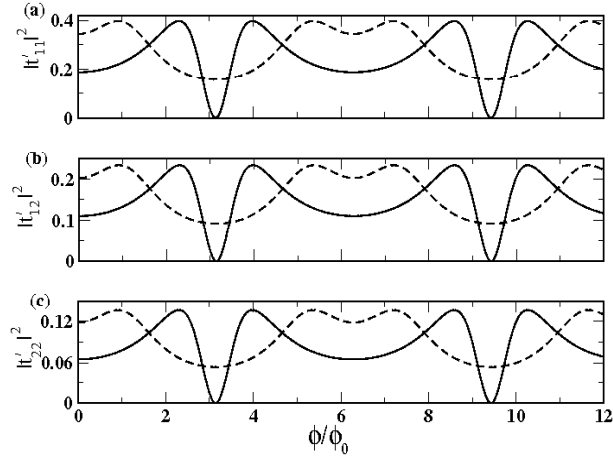


FIG. 4: We use same parameters as in Fig. 3 and plot individual scattering cross sections. (a) shows a plot of  $|t'_{11}|^2$  as a function of  $\phi/\phi_0$ . (b) shows a plot of  $|t'_{12}|^2$  as a function of  $\phi/\phi_0$ .  $|t'_{21}|^2$  as a function of  $\phi/\phi_0$  is identical to  $|t'_{12}|^2$  as a function of  $\phi/\phi_0$  due to Onsager reciprocity relation, so  $|t'_{21}|^2$  is not shown. (c) shows a plot of  $|t'_{22}|^2$  as a function of  $\phi/\phi_0$ . Here  $\phi_0 = hc/e$ . The solid lines are for  $l_1/a = 5$ ,  $l_2/a = 5$  and the dashed lines are for  $l_1/a = 4$ ,  $l_2/a = 6$ .

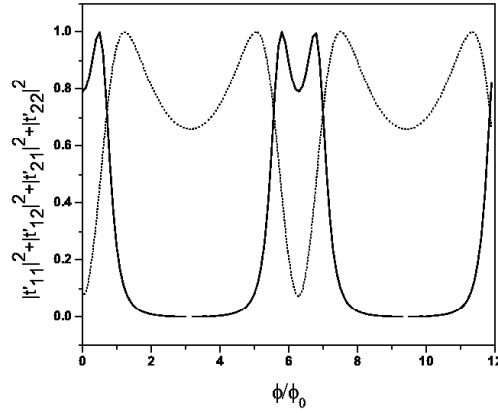


FIG. 5: The figure shows a plot of  $\sum_{i,j} |t'_{ij}|^2$  as a function of  $\phi/\phi_0$ . Here  $\phi_0 = hc/e$ . The incoming electrons have energy  $E = \frac{45\hbar^2}{m^*a^2}$ , the constant potential  $V_0$  of the ring is such that  $V_0 = \frac{10\hbar^2}{em^*a^2}$ . With this choice  $q_1$  is real and  $q_2$  is imaginary. Thus, we are considering in this case one propagating mode and one evanescent mode. The solid line is  $\sum_{i,j} |t'_{ij}|^2$  for  $l_1/a = 5$ ,  $l_2/a = 5$  and the dotted line is  $\sum_{i,j} |t'_{ij}|^2$  for  $l_1/a = 3$ ,  $l_2/a = 7$ .

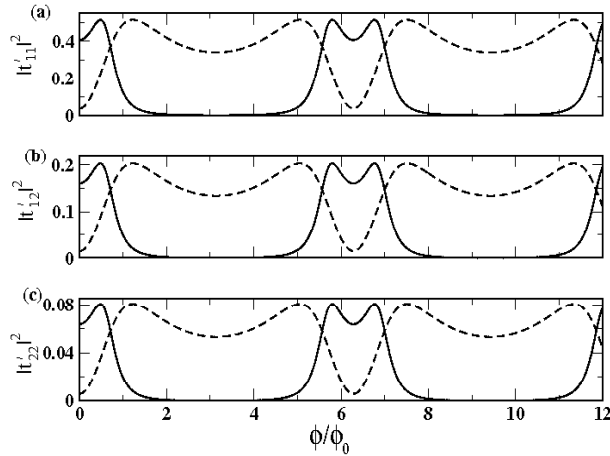


FIG. 6: We use same parameters as in Fig. 5 and plot individual scattering cross sections. (a) shows a plot of  $|t'_{11}|^2$  as a function of  $\phi/\phi_0$ . (b) shows a plot of  $|t'_{12}|^2$  as a function of  $\phi/\phi_0$ .  $|t'_{21}|^2$  as a function of  $\phi/\phi_0$  is identical to  $|t'_{12}|^2$  as a function of  $\phi/\phi_0$  due to Onsager reciprocity relation, so  $|t'_{21}|^2$  is not shown. (c) shows a plot of  $|t'_{22}|^2$  as a function of  $\phi/\phi_0$ . Here  $\phi_0 = hc/e$ . The solid lines are for  $l_1/a = 5$ ,  $l_2/a = 5$  and the dashed lines are for  $l_1/a = 3$ ,  $l_2/a = 7$ .

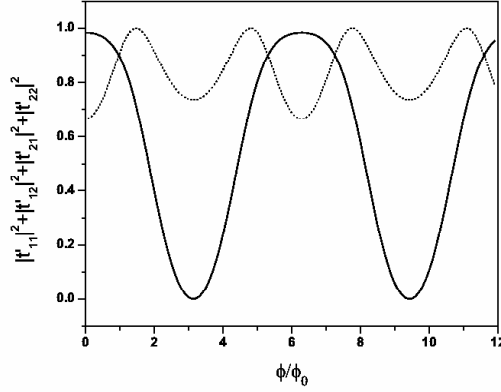


FIG. 7: The figure shows a plot of  $\sum_{i,j} |t'_{ij}|^2$  as a function of  $\phi/\phi_0$ . Here  $\phi_0 = hc/e$ . The incoming electrons have energy  $E = \frac{47\hbar^2}{m^*a^2}$ , the constant potential  $V_0$  of the ring is such that  $V_0 = \frac{10\hbar^2}{em^*a^2}$ . With this choice  $q_1$  is real and  $q_2$  is imaginary. Thus, we are considering in this case one propagating mode and one evanescent mode. The solid line is  $\sum_{i,j} |t'_{ij}|^2$  for  $l_1/a = 5$ ,  $l_2/a = 5$  and the dotted line is  $\sum_{i,j} |t'_{ij}|^2$  for  $l_1/a = 4$ ,  $l_2/a = 6$ .

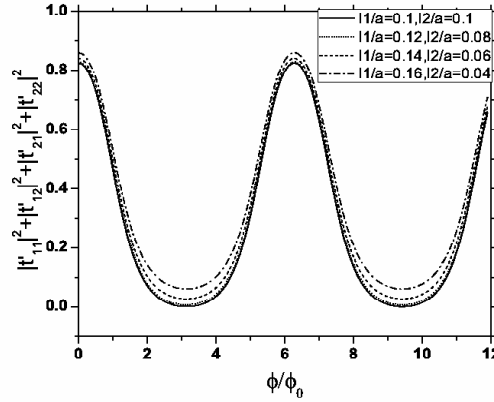


FIG. 8: The figure shows a plot of  $\sum_{i,j} |t'_{ij}|^2$  as a function of  $\phi/\phi_0$  for different arm lengths. Here  $\phi_0 = hc/e$ . The incoming electrons have energy  $E = \frac{49\hbar^2}{m^*a^2}$ . The constant potential  $V_0$  of the ring is such that  $V_0 = \frac{40\hbar^2}{em^*a^2}$ . With this choice  $q_1$  and  $q_2$  are both imaginary. Thus, we are considering in this case two evanescent modes. The exact value of  $l_1$  and  $l_2$  are given in the figure inset. For all arm length  $\sum_{i,j} |t'_{ij}|^2$  as a function of  $\phi/\phi_0$  have the same nature. That means switching action is independent of  $l_1 : l_2$ .

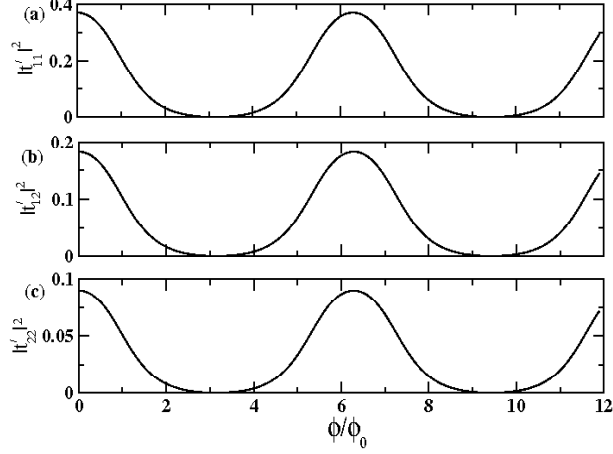


FIG. 9: We use same parameters as in Fig. 8 and plot individual scattering cross sections. (a) shows a plot of  $|t'_{11}|^2$  as a function of  $\phi/\phi_0$ . (b) shows a plot of  $|t'_{12}|^2$  as a function of  $\phi/\phi_0$ .  $|t'_{21}|^2$  as a function of  $\phi/\phi_0$  is identical to  $|t'_{12}|^2$  as a function of  $\phi/\phi_0$  due to Onsager reciprocity relation, so  $|t'_{21}|^2$  is not shown. (c) shows a plot of  $|t'_{22}|^2$  as a function of  $\phi/\phi_0$ . Here  $\phi_0 = hc/e$ . The solid lines are for  $l_1/a = 0.1$ ,  $l_2/a = 0.1$ .

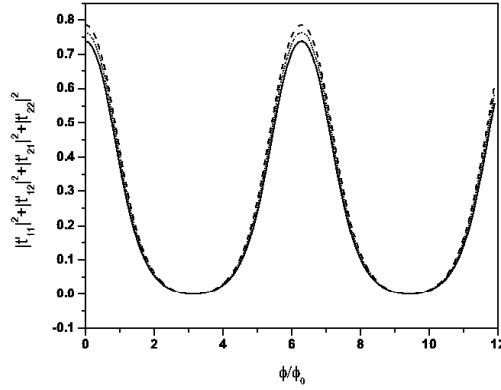


FIG. 10: The figure shows a plot of  $\sum_{i,j} |t'_{ij}|^2$  as a function of  $\phi/\phi_0$  for different incoming energy. Here  $\phi_0 = hc/e$ . The constant potential  $V_0$  of the ring is such that  $V_0 = \frac{40\hbar^2}{em^*a^2}$ . With this choice  $q_1$  and  $q_2$  are both imaginary. Thus, we are considering in this case two evanescent modes. The solid line is  $\sum_{i,j} |t'_{ij}|^2$  for  $E = \frac{45\hbar^2}{m^*a^2}$ . The dotted line is  $\sum_{i,j} |t'_{ij}|^2$  for  $E = \frac{46\hbar^2}{m^*a^2}$ . The dashed line is  $\sum_{i,j} |t'_{ij}|^2$  for  $E = \frac{47\hbar^2}{m^*a^2}$ . For all energy values  $\sum_{i,j} |t'_{ij}|^2$  as a function of  $\phi/\phi_0$  have the same nature. That means switching action is independent of incident energy.

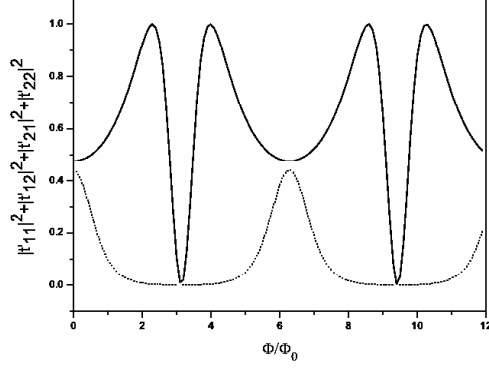


FIG. 11: The figure shows a plot of  $\sum_{i,j} |t'_{ij}|^2$  as a function of  $\phi/\phi_0$  for two choice of total ring lengths. Here  $\phi_0 = hc/e$ . The incoming electrons have energy  $E = \frac{45\hbar^2}{m^*a^2}$ , the constant potential  $V_0$  of the ring is 0. With this choice  $q_1$  and  $q_2$  are both real. Thus, we are considering in this case two propagating modes. The solid line is  $\sum_{i,j} |t'_{ij}|^2$  for  $L/a = 10$  ( $l_1/a = 5$ ,  $l_2/a = 5$ ) and the dashed line is  $\sum_{i,j} |t'_{ij}|^2$  for  $L/a = 8$  ( $l_1/a = 4$ ,  $l_2/a = 4$ ).

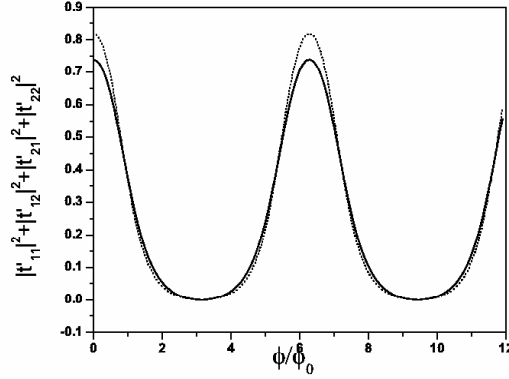


FIG. 12: The figure shows a plot of  $\sum_{i,j} |t'_{ij}|^2$  as a function of  $\phi/\phi_0$ . Here  $\phi_0 = hc/e$ . The incoming electrons have energy  $E = \frac{45\hbar^2}{m^*a^2}$ , the constant potential  $V_0$  of the ring is such that  $V_0 = \frac{40\hbar^2}{em^*a^2}$ . With this choice  $q_1$  and  $q_2$  are both imaginary. Thus, we are considering in this case two evanescent modes. The solid line is  $\sum_{i,j} |t'_{ij}|^2$  for  $L/a = 0.2$  ( $l_1/a = 0.1$ ,  $l_2/a = 0.1$ ) and the dashed line is  $\sum_{i,j} |t'_{ij}|^2$  for  $L/a = 0.16$  ( $l_1/a = 0.08$ ,  $l_2/a = 0.08$ ).